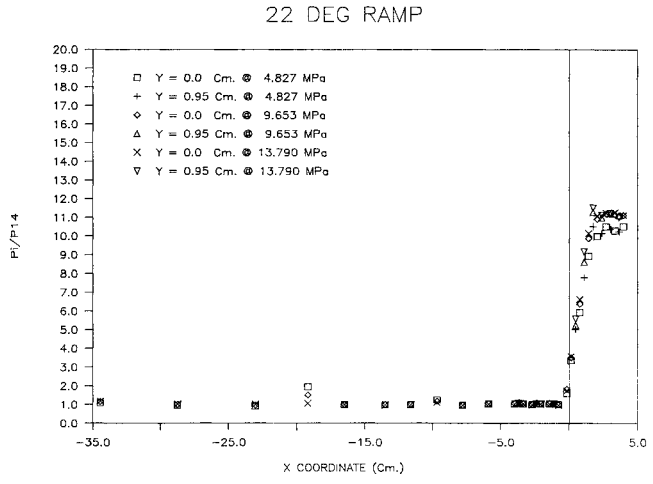

Fig. 3 Static pressure distributions on a flat plate with 22 deg ramp combination.

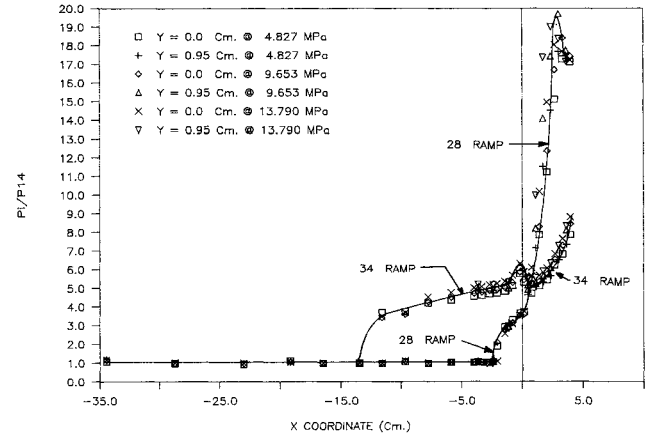

Fig. 4 Static pressure distribution on a flate plate with 28 deg ramp and 34 deg ramp.

on the upstream location of the separation point becomes apparent. That is, at a constant Reynolds number, as the adverse pressure gradient is increased the position of the interaction region moves upstream. For example, in the low unit *Re* case, as the ramp angle was increased from 22 deg to 28 deg, the separtion point moved from -2.0 mm to -20.3 mm, which indicates a change by a factor of 10. Similarly, when the angle was changed from 28 deg to 34 deg, the separation length increased by a factor of 60 to approximately -12.7 cm.

The upstream movement of the interaction region at various unit *Re* and at a fixed ramp angle indicate a critical state has been achieved. Specifically, increases in unit *Re* from 33 to 98 million/meter did not appear to significantly affect the location of the separation point. Because of the subjective nature of determining the point separation, Figs. 3 and 4 are included to demonstrate this asymptotic state, whereby the separation point as indicated by the surface pressure distribution does not appear to be noticeably different over the range of unit *Re* numbers tested.

Similar experimental results were weakly observed by Todisco and Reeves[6] for unit *Re* between approximately 33 and 49 million/meter at Mach number 6.5. Further, a closer examination of previous supersonic studies[15] appears to indicate that an asymptotic state may also be approached when the unit *Re* in their studies were increased to 82 or 98 million/meter.

In summary, the present work appears to indicate that the extent of separation is independent of Reynolds number in the range tested. That is, for unit Reynolds numbers between 23 and 98 million/meter the upstream location of the separation line appears to have reached an asymptotic state and is relatively unaffected by increases in Reynolds number.

References

[1]Roshko, A. and Thomke, G. J., "Flare-Induced Interaction Lengths in Supersonic, Turbulent Boundary Layers," *AIAA Journal,* Vol. 14, July 1976, pp. 873-879.

[2]Hunter, L. G. and Reeves, B. L., "Results of a Strong Interaction, Wake-Like Model of Supersonic Separated and Reattaching Turbulent Flows," AIAA Paper 71-128, New York, 1971.

[3]Roshko, A. and Thomke, G. J., "Supersonic Turbulent Boundary Layer Interaction with a Compression Corner at Very High Reynolds Number," *Proceedings of the Symposium on Viscous Interaction Phenomena in Supersonic and Hypersonic Flow,* USAF Aerospace Research Labs, Wright Patterson AFB, Ohio University of Dayton Press, 1969, pp. 109-138.

[4]Law, C. H., "Supersonic, Turbulent Boundary Layer Separation," *AIAA Journal,* Vol. 12, June 1974, pp. 794-797.

[5]Bogdonoff, S. M., Vas, I. E., Settles, G. S., and Simpess, G. "Research on Supersonic Turbulent Separated and Reattached Flows" Aerospace Research Lab Final Report, ARL 75-0220, June 1975.

[6]Todisco, A. and Reeves, B. L., "Turbulent Boundary Layer Separation and Reattachment at Supersonic and Hypersonic Speeds," *Proceedings of the Symposium on Viscous Interaction Phenomena in Supersonic and Hypersonic Flow,* USAF Aerospace Research Labs, Wright-Patterson AFB, Ohio, University of Dayton Press, 1969, pp. 139-179.

[7]Elfstrom, G. M., "Turbulent Hypersonic Flow at a Wedge Compression Corner," *Journal of Fluid Mechanics,* Vol. 53, Pt. 1, 1972, pp. 113-127.

[8]Spaid, F. W. and Frishett, J. C., "Incipient Separation of a Supersonic, Turbulent Boundary Layer, Including Effects of Heat Transfer," *AIAA Journal,* Vol. 10, July 1972, pp. 915-922.

[9]Fiore, A. W. and Law, C. H., "Aerodynamic Calibration of the Aerospace Research Laboratories M#6 High Reynolds Number Facility," USAF, Aerospace Research Laboratory Final Report, ARL TR 75-0028, Feb. 1975.

Mechanism of Sidewall Effect Studied with Oil Flow Visualization

Yaoxi Su*
Northwestern Polytechnical University, Xian, China

Nomenclature

M = Mach number
S = entropy
T = temperature
$\bar{u}$ = velocity vector
α = angle of attack
$\bar{\omega}$ = vorticity vector

Introduction

SIDEWALL effect has been one of the major uncertainties in airfoil experiments. In contrast with the research on conventional wall interference, the sidewall problem is less investigated and remains basically unsolved. There are research efforts on the subject, theoretical as well as experimental.[1-4] The experimental works usually give only the global effect of the sidewall; so far these results have not provided a clear picture for the mechanism of the sidewall effect. On the other hand, the theoretical studies are all subjected to various assumptions. These simplifications may be necessary

Received Aug. 16, 1988; revision received Feb. 6, 1989.

*Associate Professor, Department of Aircraft Engineering.

for the analysis because of the complexity of the problem. However, they would result in serious limitations, and the results are applicable only to rather unrealistic simple flow.

It is believed that a better understanding of the mechanism of sidewall effect is essential for the progress of the research, and the visualization study of the real flow in a transonic wind tunnel would be a valuable means of acquiring the necessary information. A series of oil flow visualization and pressure distribution measurements on airfoil NPU2 were conducted in the Transonic Wind Tunnel of DFVLR, West Germany.[5] The size of the test section was 340×600 mm^2, with slotted upper and bottom walls and solid sidewalls. The model had a chord length of 100 mm and an aspect ratio of 3.4. The test Mach number was from 0.4 to 0.78, and the Reynolds number was about 3×10^6.

Oil Flow Patterns

The oil flow patterns observed in the tests fall into five categories.

1) Subcritical flow. In this case the flowfield consists of two parts: 1) main flow, a region of nearly two-dimensional attached flow, comprising most of the flowfield, and 2) corner region, a narrow region close to the sidewall with evident three-dimensionality. Inside the region two more areas can be identified. In the first area no oil streamlines can be found, only discrete, scattered oil spots. This is clearly a region of "deadair" (separation). In the second area dark and bright streaks are seen going downstream; these seem to be the feature of streamwise vortices.

The flow in the main flow region is nearly but not exactly two-dimensional. Deflection of streamlines, evidently caused by the sidewall boudary-layer growth and by the corner separation as well, can be detected. The result is equivalent to a perturbation on the boundary of the potential flow. In subsonic flow, this perturbation will spread continuously into the depth of the main flow and thus affect the measurement at the central section.

2) Supercritical attached flow (Fig. 1). The new feature here is the presence of oblique lines emanating from near the leading edge of the corner. Close inspection suggests that these lines are just weak shock waves caused by the inward deflection of the streamlines in the supersonic flow region. In supersonic flow, the sidewall disturbances propagate in the form of waves, with little loss of intensity as they proceed, and reach only part of the flowfield. As a result the flowfield is divided into several regions: 1) the region ahead of the shocks, a region of "forbidden signal" where no sidewall effect can be detected, 2) the region of strong sidewall effect, including the corner region and the region of oblique shocks, and 3) the main flow—again, a region of nearly two-dimensional flow, but its extent much reduced.

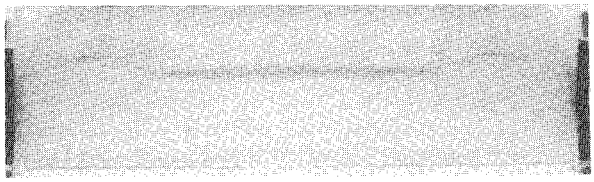

Fig. 1 Flow pattern B (supercritical attached flow), $M = 0.75$, $\alpha = 2$ deg.

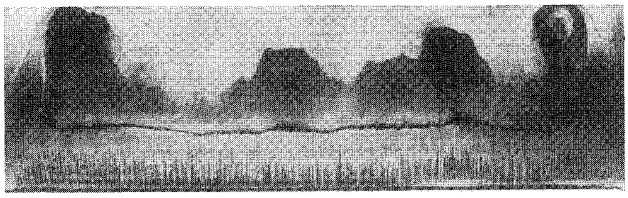

Fig. 2 Flow pattern D (supercritical flow with trailing-edge separation), $M = 0.74$, $\alpha = 6$ deg.

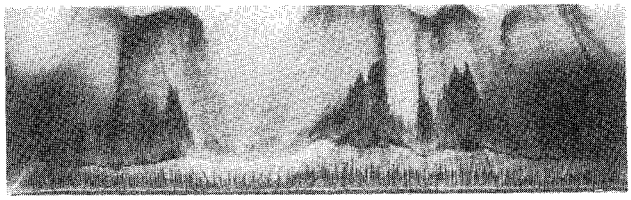

Fig. 3 Flow pattern E (highly separated flow), $M = 0.75$, $\alpha = 8$ deg.

3) Supercritical flow with local separation. The oil flow streamlines become discontinuous at the foot of the shock waves now, which means that the oil particles stop moving at the shock and the airflow separates from the surface. However, judging from the video record taken during the test, the oil flow behind normal shocks is still going downstream. Evidently this is flow with local separation and reattachment. The separation is limited spanwise in the main flow only; there is no separation in the oblique shock region.

4) Supercritical flow with trailing-edge separation (Fig. 2). Behind normal shock there is now reverse flow, as seen from video tape. Two features are distinct in the flow patttern. 1) Although the main flow has pronounced separation, the flow near the sidewall remains attached. In the oblique shock region, the adverse pressure gradient is reduced considerably. Also, the displacment effect of the sidewall boundary layer will accelerate the flow near the wall. As a result the flow is more resistant to separation near the wall. 2) A pair of large vortices appears clearly on the surface of airfoil. This may be interpreted by Crocco's theorem. Assuming that the flow is adiabatic, it follows that

$$\vec{u} \times \vec{\omega} = -T \nabla S$$

Here ∇S is the gradient of S. The theorem indicates that the three vectors $\vec{u}$, $\vec{\omega}$ and ∇S should constitute a left-hand system. Now the flow pattern has mixed attached and separated flow. In the separated flow region, dissipation of mechanical energy is stronger, and so is the entropy increment; hence, entropy gradient occurs spanwise, directed from the walls to the central section. The result is the formation of a vortex pair as seen in Fig. 2. From the kinematic point of view, the vortex is a natural transition between flows of opposite direction. The development of the oil flow pattern from local separation to trailing-edge separation does not occur simultaneously spanwise. Instead, trailing-edge separation seems to start locally from the central section. This process indicates that the trailing-edge separation in the main flow is postponed by the sidewall effect. The nearer it is to the sidewall, the later the incipience of separation.

5) Highly separated flow (Fig. 3). In this case the separated flow is highly three-dimensional. There is no longer a nearly two-dimensional flow region, even for an airfoil of large aspect ratio. There seems no reason to attribute this change of flow pattern to the sidewall effect. More likely this is due to some kind of spanwise coherent structure of turbulent separated flow. Under these circumstances the value of "two-dimensional test" is doubtful.

Development of Flow Patterns

It is found that the flow patterns change regularly with increase in Mach number and/or angle of attack from pattern A to pattern E; i.e., the pattern is decided by the two parameters M and α. More careful examination reveals that it is possible to find a single parameter that decides the flow pattern. This is the maximum local Mach number on the airfoil, i.e., the Mach number at the suction peak. The role of this parameter is readily understood because first, it decides whether the flow is subcritical or supercritical, and second, it is a measure of the intensity of the normal shock, which would decide the extent of separation.

Discussion

The sidewall effect of supercritical flow is more complicated and its influence more pronounced compared to subcritial flow cases. The disturbances of sidewall reach further because of the oblique shock waves. A narrow, "two-dimensional" wind tunnel for airfoil testing appears no longer appropriate for transonic research due to the influence of the shock. Tunnels with larger width will improve the situation a little, but there seems to be no easy solution to the problem.

At present there exist two types of physical models in the interpretation of the sidewall effect, the vortex model and the displacement model.[6] The present results strongly support the displacement model as most of the oil flow features observed can be explained satisfactorily by the model.

References

[1]Preston, J. H., "The Interference on a Wing Spanning a Closed Tunnel, Arising from the Boundary Layers on the Sidewalls, With Special Refererence to the Design of Two-Dimensional Tunnels," Aeronautical Research Council R&M 1924, March 1944.

[2]Barnwell, R. W., "A Similarity Rule of Compressibility and Sidewall Boundary Layer Effects in Two-Dimensional Wind Tunnels," AIAA Paper 79-108, Jan. 1979.

[3]Bernard-Guelle, R., "Influence of Wind Tunnel Wall Boundary on Two-Dimensional Transonic Tests," NASA TT F-17255, Nov. 1975.

[4]Murthy, A. V., Johnson, C. B., Ray, E. J., and Lawing, P. L., "Recent Sidewall Boundary-Layer Investigation with Suction in the Langley 0.3-m Transonic Cryogenic Tunnel," AIAA Paper 82-234, Jan. 1982.

[5]Friedrichs, R., and Puffert-Meissner, W., "Anstrichbilder am Profil NPU2 im Transsonischen Windkanal der DFVLR in Braunschweig (TWB)," German Aerospace Research Establishment IB 19111-86A18, Sept. 1986.

[6]Chevallier, J. P., "Three-Dimensional Effects on Airfoils," NASA TM-77025, Feb. 1983.

Refinement of Higher-Order Laminated Plate Theories

K. Bhaskar* and T. K. Varadan†
Indian Institute of Technology, Madras, India

Introduction

TO account for shear deformation in composite plates by the displacement approach, a number of improved plate theories have been proposed by various authors. Starting from a Mindlin-type theory that is different from classical plate theory only in that the normal to the midplane before deformation is assumed to remain straight, not normal, after deformation, these theories have progressed to the extent of considering cubic or higher-order variation of the in-plane displacements $\bar{U}$ and $\bar{V}$ and quadratic or higher-order variation of the transverse displacement $\bar{W}$, with respect to the transverse coordinate z, and satisfaction of zero shear condition on the lateral surfaces of the plate. However, the transverse shear and normal stress continuity at interfaces of the laminate is generally violated. The aim of the present note is to indicate how transverse shear stress continuity can also be incorporated without increasing the number of unknown variables by using a piecewise displacement distribution. This is illustrated with reference to a particular displacement model used in Ref. 1.

Piecewise variation of $\bar{U}$ and $\bar{V}$, with respect to z represents well the behavior of the laminate wherein the stiffness varies drastically at an interface. This has been used earlier,[2,3] but such analyses have been confined to theories of the Mindlin type and consequently violate the zero shear condition on lateral surfaces. The present anaysis considers symmetric laminates subjected to antisymmetric loading about the midplane.

Formulation

A symmetric laminate of total thickness $2h$ made up of $2N$ specially orthotropic laminae is considered. The reference surface $z = 0$ is taken at the midplane, and the layers in the positive z direction are numbered serially from 1 to N starting from the layer nearest to $z = 0$. The constitutive law for the kth layer is assumed as

$$\begin{Bmatrix} \sigma_x \\ \sigma_y \\ \sigma_z \end{Bmatrix}^{(k)} = \begin{bmatrix} C_{11} & C_{12} & C_{13} \\ C_{12} & C_{22} & C_{23} \\ C_{13} & C_{23} & C_{33} \end{bmatrix}^{(k)} \begin{Bmatrix} \epsilon_x \\ \epsilon_y \\ \epsilon_z \end{Bmatrix}^{(k)} \tag{1a}$$

$$\begin{Bmatrix} \tau_{yz} \\ \tau_{xz} \\ \tau_{xy} \end{Bmatrix}^{(k)} = \begin{bmatrix} C_{44} & 0 & 0 \\ 0 & C_{55} & 0 \\ 0 & 0 & C_{66} \end{bmatrix}^{(k)} \begin{Bmatrix} \gamma_{yz} \\ \gamma_{xz} \\ \gamma_{xy} \end{Bmatrix}^{(k)} \tag{1b}$$

The displacement model is chosen, for $z \geq 0$, as

$$\bar{U}(x,y,z) = -zW_{,x} - pu + \sum_{k=1}^{N-1} \phi_k [p - p(z_k)] H(z - z_k) \tag{2a}$$

$$\bar{V}(x,y,z) = -zW_{,y} - pv + \sum_{k=1}^{N-1} \psi_k [p - p(z_k)] H(z - z_k) \tag{2b}$$

$$\bar{W}(x,y,z) = W + qw \tag{2c}$$

$$\bar{U}, \bar{V}(x,y,-z) = -\bar{U}, \bar{V}(x,y,z) \tag{2d}$$

$$\bar{W}(x,y,-z) = \bar{W}(x,y,z) \tag{2e}$$

$$p = p(z) = z - (z^3/3h^2) \tag{2f}$$

$$q = q(z) = 1 - (z^2/h^2) \tag{2g}$$

where W, w, u, v, ϕ_k, and ψ_k are functions of x,y only, $H(z - z_k)$ is the Heaviside Unit step function, and the summation in u and v is extended over the $(N - 1)$ interfaces, the kth interface being defined as that between the kth and $(k + 1)$th laminae. The variation of $\bar{W}$ with z is small and hence is assumed to be the same for all layers. In the absence of terms containing ϕ_k and ψ_k, this displacement variation is the same as that used in Ref. 1.

It can be seen that this distribution satisfies displacement compatibility at interfaces and the zero shear condition on lateral surfaces of the plate. By enforcing shear stress continuity at interfaces, ϕ_k and ψ_k can be obtained as

$$\phi_k = r_k(-u + w_{,x}),\ \psi_k = s_k(-v + w_{,y}),$$

$$k = 1 \text{ to } (N - 1) \tag{3a}$$

$$r_k = \left[\frac{C_{55}^{(k)}}{C_{55}^{(k+1)}} - 1\right]\left(1 + \sum_{p=1}^{k-1} r_p\right)$$

$$k = 2 \text{ to } (N - 1) \tag{3b}$$

Received Jan. 25, 1989; revision received March 1, 1989.

*Research Scholar, Department of Aerospace Engineering.
†Professor, Department of Aerospace Engineering.